Observation of Relativistic and Charge-Displacement Self-Channeling of Intense Subpicosecond Ultraviolet (248 nm) Radiation in Plasmas

A. B. Borisov,[1] A. V. Borovskiy,[2] V. V. Korobkin,[2] A. M. Prokhorov,[2] O. B. Shiryaev,[1] X. M. Shi,[3] T. S. Luk,[3] A. McPherson,[3] J. C. Solem,[4] K. Boyer,[3] and C. K. Rhodes[3]

[1]*Laboratory for Computer Simulation, Research Computer Center, Moscow State University, Moscow, 119899, Russia*
[2]*General Physics Institute, Academy of Sciences of Russia, Moscow, 117942, Russia*
[3]*Department of Physics, University of Illinois at Chicago, Chicago, Illinois 60680*
[4]*Theoretical Division, Los Alamos National Laboratory, Los Alamos, New Mexico 87545*
(Received 13 November 1991)

Experimental studies examining a new relativistic regime of high-intensity short-pulse propagation in plasmas have been performed which present evidence for the formation of a stable mode of spatially confined (channeled) propagation. For an electron density of $\sim 1.35\times10^{21}$ cm^{-3} and a power of $\sim 3\times10^{11}$ W, the results indicate a channel radius < 1 μm and a peak intensity $\sim 10^{19}$ W/cm^2. Comparison of these findings with a dynamical theory yields agreement for both the longitudinal structure and the radial extent of the propagation observed.

PACS numbers: 52.40.Db, 42.25.−p, 42.65.Jx

A fundamentally new regime of electromagnetic propagation is expected to arise in plasmas for short-pulse radiation at sufficiently high intensity. Calculations of the propagation in plasmas, incorporating both relativistic [1,2] and charge-displacement mechanisms [3–7], indicate that the combined action of these processes can lead to a new stable form of spatially confined (channeled) propagation. This Letter (1) reports the results of the first experimental study probing the physical regime relevant to the observation of relativistic and charge-displacement self-channeling and (2) presents the initial comparison of these experimental findings with matching theoretical calculations performed with the computational procedures described in Ref. [7].

The experimental arrangement used in these studies is illustrated in Fig. 1(a). The source of radiation was a subpicosecond KrF* ($\lambda = 248$ nm) laser that has been described elsewhere [8]. It delivered a linearly polarized power of $\sim 3\times10^{11}$ W ($\sim$150 mJ, pulse duration $\sim$500 fs) in a beam with a diameter of $\sim$42 mm. When this radiation was focused into the chamber with lens $L1$ ($f/7$), a focal radius $r_0 \sim 3.5$ μm was measured, giving a maximum intensity $I_0 \sim 8.6\times10^{17}$ W/cm^2. The medium was provided by filling the chamber statically with gas [He, Ne, Ar, Kr, Xe, N_2, CO_2, or a mixture of Xe (4%) and N_2 (96%)] up to a maximum density of $\sim 1.89\times10^{20}$ cm^{-3}.

The diffracted 248-nm radiation was measured as a function of the angle (Θ) with respect to the direction of the incident radiation. The incident laser beam was blocked by a metal disk on the output window of the chamber and lens $L2$ imaged the region near the focal zone on a fluorescent screen S. The diaphragm D in front of lens $L2$ restricted the collection of the diffracted light to a solid angle of $\sim 5°$ while simultaneously increasing the depth of field. The angle between the axis of the lens $L2$ and the axis of the incoming laser radiation could be readily varied up to a maximum angle of $\Theta \sim 15°$. Two flat mirrors coated for high reflection ($\sim$99%) at 248 nm, both having a spectral bandwidth of $\sim$10 nm, served in reflection as spectral filters (F) for the diffracted laser radiation so that only the scattered 248-nm radiation could illuminate the screen. An attenuator A was employed to adjust the intensity on the screen and the images formed were recorded through the visible fluores-

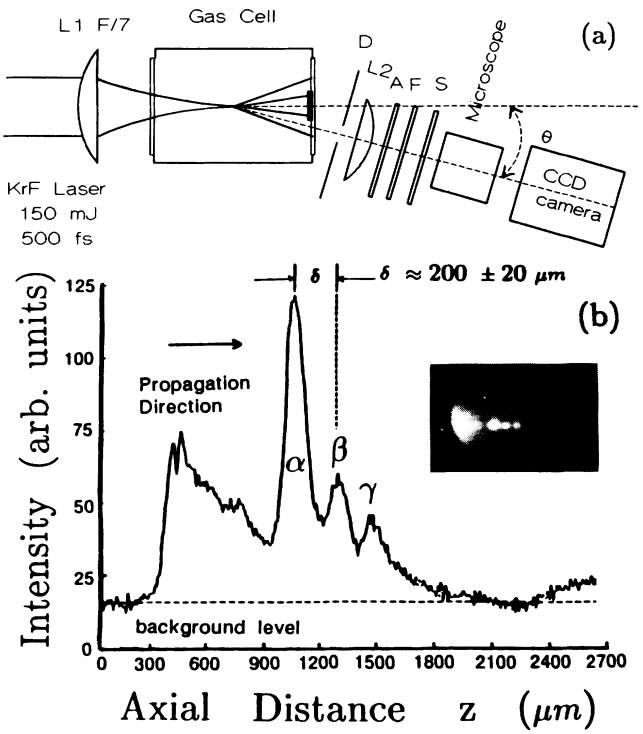

FIG. 1. (a) Experimental apparatus used in studies of propagation. See text for description. (b) Data concerning the pattern of propagation observed with a single pulse in N_2 at a density of $\sim 1.35\times10^{20}$ cm^{-3}. The maximum intensity is half the detector (CCD) saturation. The radiation is incident from the left. Inset: Photographic data with a vertical spatial resolution of $\sim$10 μm. The graph illustrates the one-dimensional axial profile taken along the direction of propagation (z) of the photographic data (inset). The spacing of the maxima, $\delta \simeq 200 \pm 20$ μm, is indicated.

cence produced with a microscope and a charge-coupled-device (CCD) camera.

The characteristic behavior observed is well illustrated by the data recorded with N_2. The measured result, shown in Fig. 1(b), corresponds to a density $\rho_{N_2} \sim 1.35 \times 10^{20}$ cm^{-3}. To the left, in the photographic inset, a relatively large cone of light Rayleigh scattered from the plasma is visible at all angles as the energy propagates toward the focal point of the lens, while, in the region to the right of the conical apex, a narrow filament developed. The diameter of this filament is not greater than 10 μm, the measured spatial resolution of the imaging system. The distribution of intensity observed along the filament exhibited several bright features attributed to diffraction because they could not be seen for $\Theta > 20°$. Since the axis of the imaging lens corresponded to an angle $\Theta = 7.5°$, the scale along the abscissa of the photographic data is reduced by almost eightfold, giving the maximum length of the filament as ~ 1 mm. The graph in Fig. 1(b) represents a one-dimensional axial profile, taken along the direction of propagation (z), of the observed intensity pattern (inset). Three peaks (α, β, γ) are visible with a a spatial separation of $\delta = 200 \pm 20$ μm. The normal Rayleigh range for the focal geometry used was ~ 200 μm.

The diameter of the filamentary channel is an important dynamical variable, which we estimated by measuring the maximum angular deviation of the diffracted light. The experimental value ϕ of this diffracted cone was $\phi \sim 20°$, a magnitude indicating a radius $r_\phi \sim 0.9$ μm though the relation $\phi = 1.22\lambda/r_\phi$. Filaments of this general nature were observed at densities above $\sim 1.35 \times 10^{20}$ cm^{-3} in N_2, Ne, Ar, Kr, CO_2, and a mixture of Xe (4%) and N_2 (96%), but not in He and Xe, two materials discussed further below.

Two mechanisms exist that could modify the refractive index of the medium and lead to the observed behavior. They are (1) the Kerr effect stemming from the ions and (2) the relativistic and charge-displacement process [7]. Since the pulse duration is very short (~ 500 fs), the motion of the ions is negligible [3], and no contribution can arise from expulsion of the plasma from the high-intensity zone. An implication of the estimate of the channel radius ($r_\phi \sim 0.9$ μm) is that the observed propagation is associated with intensities in the 10^{18}–10^{19} W/cm^2 range. Under these conditions, available experimental evidence [9,10] on multiphoton ionization indicates that He should be fully ionized and the C, N, and O atoms constituting the molecular materials would retain, at most, only $1s$ electrons.

Consider explicitly the case of N_2, which has estimated [9,10] threshold intensities for the production of N^{5+}, N^{6+}, and N^{7+} of 1.6×10^{16}, 6.4×10^{18}, and 1.3×10^{19} W/cm^2, respectively. Hence, the volume of the channel would be largely ionized to N^{5+}, with certain localized high-intensity regions contributing some N^{6+}. Two consequences of this pattern of ionization follow, namely, (i) the Kerr effect arising from the ions is small, since the polarizabilities of the remaining $1s$ electrons are low, and (ii) the electron density (n_e) initially produced in the focal region is nearly uniform. Therefore, $n_e \simeq 1.35 \times 10^{21}$ cm^{-3} for the data on N_2 shown in Fig. 1(b).

A critical power P_{cr} for self-channeling, arising from the relativistic and charge-displacement mechanism, can be defined [11] as

$$P_{cr} = (m_e^2 c^5/e^2) \int_0^\infty g_0^2(r) r\, dr (\omega/\omega_{p,0})^2 \simeq 1.62 \times 10^{10} (n_{cr}/n_e)\ \mathrm{W}, \quad (1)$$

where m_e, e, and c have their customary identifications, ω is the laser angular frequency, $\omega_{p,0}$ is the plasma frequency for the uniform unperturbed plasma with electron density n_e, n_{cr} is the critical electron density (for $\lambda = 248$ nm, $n_{cr} = 1.82 \times 10^{22}$ cm^{-3}), and $g_0(r)$ is the Townes mode [12].

The critical powers associated with the experimental conditions, for He and N_2 at a medium density $\rho = 1.35 \times 10^{20}$ cm^{-3}, are 1.08×10^{12} and 2.19×10^{11} W, respectively. Therefore, since the incident power was $P \simeq 3 \times 10^{11}$ W, no filament was expected in He, a prediction conforming with the observation of none. Moreover, the diffracted cone of radiation was also absent with He. In contrast, $P/P_{cr} \simeq 1.37$ for N_2, a condition that held generally ($P/P_{cr} > 1$) for all materials which exhibited evidence for channel formation. We note, however, that some contribution from the Kerr effect may be present, even for the light materials (Ne, N_2, and CO_2), in the early stage of channel formation prior to the development of a substantial level of ionization, and that the heavier gases (Ar, Kr, and Xe) may involve a more significant influence from the Kerr process. A specific estimate of the nonlinear index change arising from both N^{5+} and N^{6+} at an intensity of $\sim 10^{19}$ W/cm^2 indicates that their contribution is less than 10^{-3} that of the free electrons; hence the ionic contribution can be neglected in N_2 for the conditions studied.

A direct comparison will now be made between the theoretical analysis, fully described in Ref. [7], and the experimental findings for N_2. This comparison can be accomplished for both the longitudinal intensity profile and the radial extent of the channel. Figure 2(a) illustrates the intensity profile $I(r,z)/I_0$ calculated with physical parameters corresponding to those of the experiment (i.e., $P \simeq 3 \times 10^{11}$ W, $r_0 = 3.5$ μm, $n_e = 1.35 \times 10^{21}$ cm^{-3}, and $P/P_{cr} = 1.37$). Importantly, *all* of these parameters are based on *independent* measurements of (1) the laser pulse involving determinations of the energy and power (P), (2) the focal radius (r_0) of the incident radiation, and (3) the characteristics of the multiphoton ionization [10] generating the electron density (n_e). Therefore, this comparison does *not* involve a fit with a free parameter. The normalized electron density calculated is presented in Fig. 2(b), from which it is seen that electronic cavitation occurs only near the positions of the maxima in the intensity profile [Fig. 2(a)]. Curve A in Fig. 2(c) represents

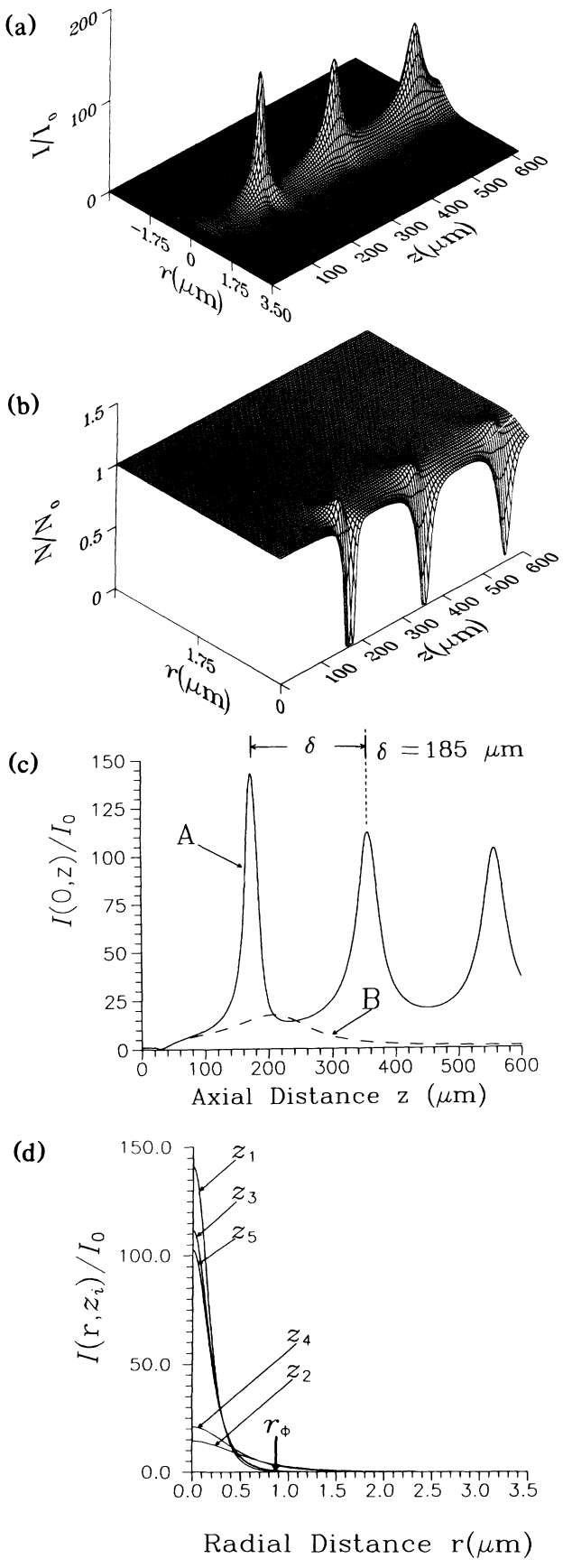

the one-dimensional axial intensity profile $I(0,z)/I_0$ corresponding to the calculated distribution shown in Fig. 2(a). The spacing (δ) of the maxima is seen to be $\delta \sim 185$ μm, a value in close agreement with the experimental figure ($\delta = 200 \pm 20$ μm) illustrated in Fig. 1(b). Furthermore, analysis has shown that the spacing δ is quite sensitive to the power P_0 and electron density n_e, particularly in the region close to the threshold [see Eq. (1)]. With respect to the results illustrated in Fig. 2(c), an increase in n_e by less than 5% causes a reduction in the spacing δ by approximately 25%. Therefore, substantial changes in the physical parameters would grossly alter the comparison of the experimental and theoretical results.

Theoretical studies [3-7,11] indicate that the charge displacement plays a very important dynamical role. In order to test this hypothesis, identical calculations were made for N_2 for the purely relativistic case [2] which explicitly neglects the charge-displacement term, namely, elimination of the term $(c^2/\omega_{p,0}^2 r_0^2)\Delta_\perp (1+I/I_r)^{1/2}$ in Eq. (24) of Ref. [7]. Significantly, the resulting axial profile [curve *B* in Fig. 2(c)] exhibits only a *single* relatively weak maximum, for $0 \leq z \leq 600$ μm, an outcome sharply at variance with both the full theoretical analysis and the experimental observation. Although the expected charge displacement is highly localized [Fig. 2(b)], this comparison reveals the strong influence it has on the propagation [3,7,11]. At a greater incident power ($P/P_{cr} \sim 10$), a continuous channel in the electron distribution is expected to develop [7].

The measurements indicated an approximate value of $r_\phi \simeq 0.9$ μm for the radial extent of the channel, a result that can be compared with the corresponding theoretical figure. Figure 2(d) illustrates five radial intensity profiles $I(r,z_i)/I_0$ of the distribution pictured in Fig. 2(a). Since the measurement of this angularly scattered radiation did not correspond to a known longitudinal position, this comparison can only be qualitative, but the radial distributions shown indicate that the expected value lies in the interval $0.5 \leq r \leq 1.0$ μm, a range that comfortably includes the experimental value r_ϕ.

The results observed with Xe deserve additional discussion, since those experiments did not give evidence for the formation of a channel. In significant contrast to the case involving N_2, the electron density n_e produced by the multiphoton ionization [10] in Xe is expected to be very

FIG. 2. Calculations for N_2 with $P = 3\times10^{11}$ W, $r_0 = 3.5$ μm, $n_e = 1.35\times10^{21}$ cm^{-3}, and $I_0 = 8.6\times10^{17}$ W/cm^2. (a) Normalized intensity $I(r,z)/I_0$. (b) Normalized electron density $N(r,z)/N_0$ for N_2 with $N_0 = n_e$. (c) Normalized one-dimensional axial intensity profiles $I(0,z)/I_0$. Curve *A*, full theory for data in panel (a), $\delta = 185$ μm. Curve *B*, calculation with charge-displacement term neglected. (d) Normalized radial intensity profiles $I(r,z_i)/I_0$ corresponding to panel (a). Longitudinal positions $z_1 = 172$ μm, $z_2 = 245$ μm, $z_3 = 358$ μm, $z_4 = 441$ μm, and $z_5 = 559$ μm and $r_\phi = 0.9$ μm.

nonuniform spatially. For intensities spanning 10^{16}–10^{18} W/cm^2, the corresponding density n_e would vary by over a factor of 2. Since this nonuniformity would tend to reduce the refractive index locally in the central high-intensity region, a significant defocusing action is expected which could suppress the channel formation.

Finally, we note (1) that the intensity distribution is not expected to depend strongly on the state of polarization [13,14] and (2) that losses to the plasma may be significant, particularly at electron densities close to n_{cr}.

The first experiments examining a new relativistic regime of high-intensity pulse propagation in plasmas have been performed and the findings indicate the formation of a channeled mode of propagation over a length considerably greater than the Rayleigh range. Specific comparisons of the experimental observations with a dynamical theory, which explicitly includes both the influence of the relativistic mass shift and the displacement of the electronic component of the plasma, produce excellent agreement for both the longitudinal structure of the intensity profile and the radial extent of the channel. While the present channel contains several foci, a continuous channel is predicted to develop at higher power. Finally, the intrinsically very high concentration of power associated with this mechanism of channeled propagation provides an efficient and general method for the production of conditions necessary for x-ray amplification [15].

The authors acknowledge the expert technical assistance of J. Wright and P. Noel in addition to fruitful conversations with A. R. Hinds, R. R. Goldstein, and B. Bouma. Support for this research was partially provided under Contracts No. AFOSR-89-0159, (ONR) No. N00014-91-J-1106, (SDI/NRL) No. N00014-91-K-2013, (ARO) No. DAAL 3-91-G-0174, (DOE) No. DE-FG02-91ER12108, and (NSF) No. PHY-9021265.

[1] C. Max, J. Arons, and A. B. Langdon, Phys. Rev. Lett. **33**, 209 (1974).

[2] A. B. Borisov, A. B. Borovskiy, V. V. Korobkin, A. M. Prokhorov, C. K. Rhodes, and O. B. Shiryaev, Phys. Rev. Lett. **65**, 1753 (1990).

[3] J. C. Solem, T. S. Luk, K. Boyer, and C. K. Rhodes, IEEE J. Quantum Electron. **25**, 2423 (1989).

[4] P. Sprangle, E. Esarey, and A. Ting, Phys. Rev. Lett. **64**, 2011 (1990); P. Sprangle, C. M. Tang, and E. Esarey, Phys. Rev. A **41**, 4463 (1990); A. Ting, E. Esarey, and P. Sprangle, Phys. Fluids B **2**, 1390 (1990).

[5] G. Z. Sun, E. Ott, Y. C. Lee, and P. Guzdar, Phys. Fluids **20**, 526 (1987).

[6] T. Kurki-Suonio, P. J. Morrison, and T. Tajima, Phys. Rev. A **40**, 3230 (1989).

[7] A. B. Borisov, A. V. Borovskiy, O. B. Shiryaev, V. V. Korobkin, A. M. Prokhorov, J. C. Solem, T. S. Luk, K. Boyer, and C. K. Rhodes, Phys. Rev. A (to be published).

[8] T. S. Luk, A. McPherson, G. Gibson, K. Boyer, and C. K. Rhodes, Opt. Lett. **14**, 1113 (1989).

[9] S. Augst, D. Strickland, P. D. Meyerhofer, S. L. Chin, and J. H. Eberly, Phys. Rev. Lett. **63**, 2212 (1989).

[10] G. Gibson, T. S. Luk, and C. K. Rhodes, Phys. Rev. A **41**, 5049 (1990).

[11] A. B. Borisov, A. V. Borovskiy, V. V. Korobkin, A. M. Prokhorov, O. B. Shiryaev, and C. K. Rhodes, J. Laser Phys. **1**, 103 (1991).

[12] R. Y. Chiao, E. Garmire, and C. H. Townes, Phys. Rev. Lett. **13**, 479 (1964).

[13] P. Avan, C. Cohen-Tannoudji, J. Dupont-Roc, and C. Fabre, J. Phys. (Paris) **37**, 993 (1976).

[14] S. V. Bulanov, V. I. Kirsanov, and A. S. Sakharov, Fiz. Plazmy **16**, 935 (1990) [Sov. J. Plasma Phys. **16**, 543 (1990)].

[15] K. Boyer, A. B. Borisov, A. V. Borovskiy, O. B. Shiryaev, D. A. Tate, B. E. Bouma, X. M. Shi, A. McPherson, T. S. Luk, and C. K. Rhodes, "Method of Concentration of Power in Materials for X-Ray Amplification" (to be published).

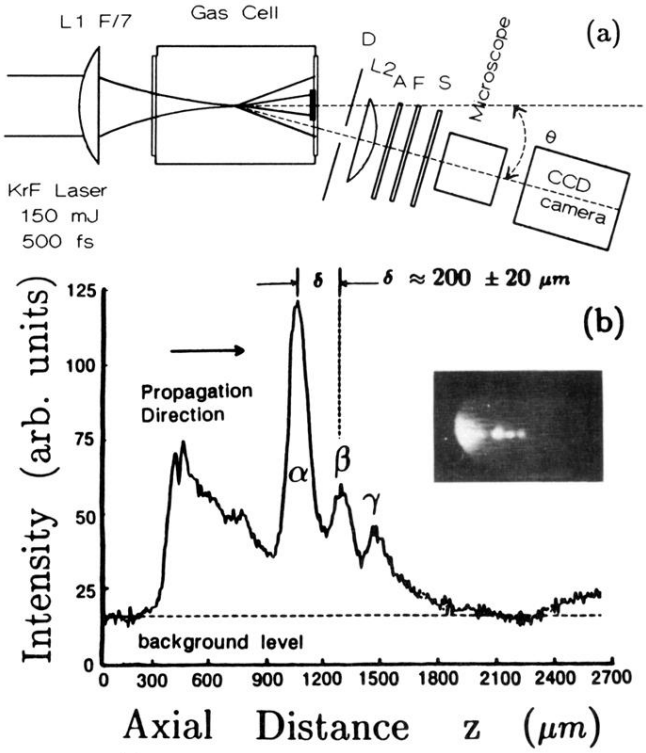

FIG. 1. (a) Experimental apparatus used in studies of propagation. See text for description. (b) Data concerning the pattern of propagation observed with a single pulse in N_2 at a density of $\sim 1.35 \times 10^{20}$ cm^{-3}. The maximum intensity is half the detector (CCD) saturation. The radiation is incident from the left. Inset: Photographic data with a vertical spatial resolution of ~ 10 μm. The graph illustrates the one-dimensional axial profile taken along the direction of propagation (z) of the photographic data (inset). The spacing of the maxima, $\delta \simeq 200 \pm 20$ μm, is indicated.

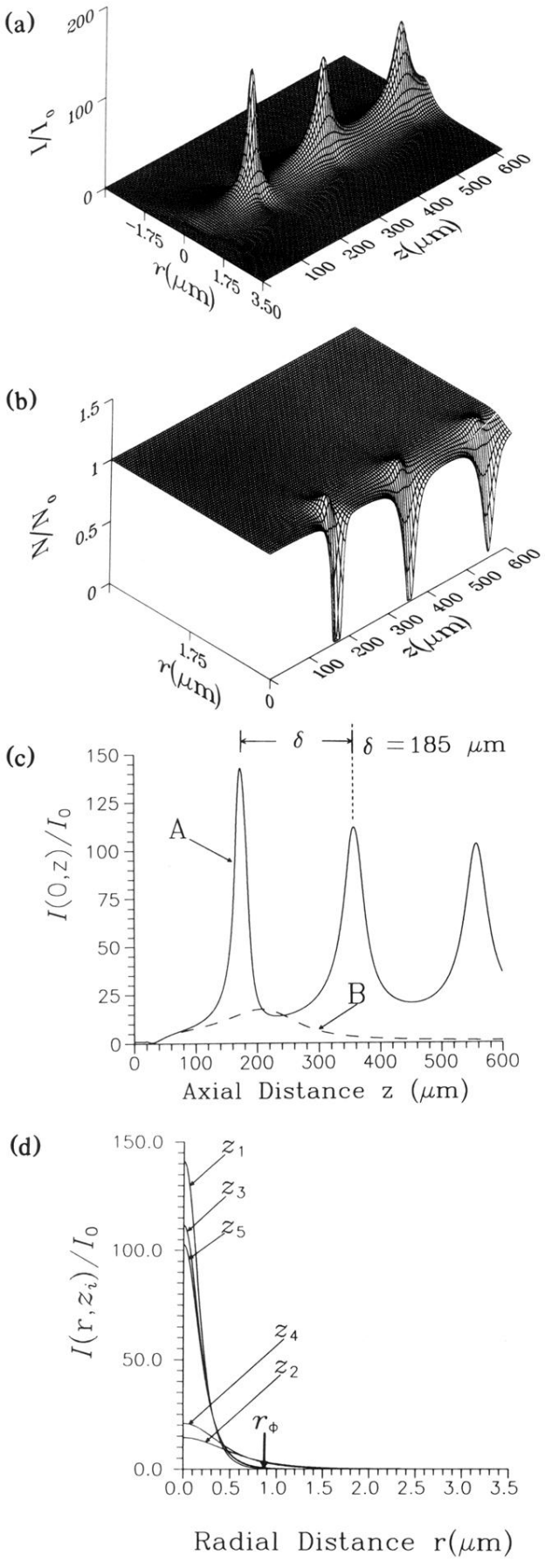

FIG. 2. Calculations for N_2 with $P=3\times10^{11}$ W, $r_0=3.5$ μm, $n_e=1.35\times10^{21}$ cm^{-3}, and $I_0=8.6\times10^{17}$ W/cm^2. (a) Normalized intensity $I(r,z)/I_0$. (b) Normalized electron density $N(r,z)/N_0$ for N_2 with $N_0=n_e$. (c) Normalized one-dimensional axial intensity profiles $I(0,z)/I_0$. Curve *A*, full theory for data in panel (a), $\delta=185$ μm. Curve *B*, calculation with charge-displacement term neglected. (d) Normalized radial intensity profiles $I(r,z_i)/I_0$ corresponding to panel (a). Longitudinal positions $z_1=172$ μm, $z_2=245$ μm, $z_3=358$ μm, $z_4=441$ μm, and $z_5=559$ μm and $r_\phi=0.9$ μm.